Available online at www.sciencedirect.com
ScienceDirect
Journal of Power Sources 171 (2007) 990–998
JOURNAL OF POWER SOURCES
www.elsevier.com/locate/jpowsour

Nanocrystalline TiO_2 film with textural channels: Exhibiting enhanced performance in quasi-solid/solid-state dye-sensitized solar cells

Zhigang Chen [a], Yiwen Tang [b], Hong Yang [a], Yongyao Xia [a], Fuyou Li [a,*], Tao Yi [a], Chunhui Huang [a,**]

[a] *Department of Chemistry & Laboratory of Advanced Materials, Fudan University, Handan Road 220, Shanghai 200433, PR China*
[b] *Institute of Nano-Science and Technology, Central China Normal University, Wuhan 430079, PR China*

Received 9 March 2007; received in revised form 3 July 2007; accepted 5 July 2007
Available online 10 July 2007

Abstract

Novel nanocrystalline TiO_2 films with the textural channels are obtained for dye-sensitized solar cells (DSSCs). The textural channels consisting of the cracks on the surface and the nanopores with average diameter of about 41 nm are produced by packaging ZnO nanowires with diameter of 30–50 nm into TiO_2 films and subsequently etching ZnO nanowires by hydrochloric acid. The performances of DSSCs based on novel TiO_2 films (with the textural channels) and traditional TiO_2 films (without the textural channels) are investigated, respectively. When two kinds of typical quasi-solid-state electrolytes and one kind of solid-state electrolyte are used, the energy conversion efficiencies of DSSCs from novel TiO_2 films are improved by 20–30% compared to that from traditional TiO_2 films. The reasons for the great improvement are investigated chiefly by UV–vis absorption spectra, field emission-scanning electron microscope (FE-SEM) and electrochemical impedance spectroscopy (EIS) technique. The results show that the introduction of the textural channels facilitates better penetration of quasi-solid/solid-state electrolytes into the nanopores of novel TiO_2 films and thus results in better interfacial/electrical contact and faster interfacial reaction.

Keywords: TiO_2 film; Textural channel; Dye-sensitized solar cells; Quasi-solid/solid-state electrolytes

1. Introduction

Dye-sensitized solar cells (DSSCs) have received considerable attention as a cost-effective alternative to conventional solar cells [1–7]. Above 10% light-to-electricity conversion efficiency has been achieved in DSSCs with organic solvent-based electrolyte [8]. However, the presence of organic liquid electrolytes in cells results in some problems such as leakage, evaporation of solvent, high-temperature instability and flammability. Therefore, many attempts have been made to substitute liquid electrolytes with quasi-solid/solid-state electrolytes, for example, p-type semiconductors [9], organic hole-transport materials [10,11], low molecular weight gels [12], ionic liquid-based gel electrolytes [13–16], polymer gel electrolytes [17–22], plastic crystal electrolyte [23–25] and solid polymer electrolytes [26–30]. It is well known that the interfacial contact and reaction between the dye-sensitized TiO_2 film and the electrolyte are important factors in determining the electron transfer efficiency and consequently the overall solar-to-electric conversion efficiency. Unfortunately, quasi-solid/solid-state electrolytes are difficult to penetrate into the nanopores of TiO_2 film compared with organic liquid electrolytes, which usually leads to poorer interfacial contact/reaction and lower conversion efficiencies of quasi-solid/solid DSSCs compared with those of the liquid versions. It has been reported that better wetting and pore filling of TiO_2 film by organic hole-transport materials (even having relative lower carrier mobility) can improve interfacial contact and reaction and thus cause better conversion efficiencies [31]. Therefore, to promote the interfacial contact and reaction, the wetting and pore filling of the nanoporous TiO_2 layer by the quasi-solid/solid-state electrolyte should be maximized. Some works have been done to modify quasi-solid/solid-state electrolytes, such as adding amorphous oligomer [27] or nanoparticles [7,26,30] into the electrolyte. To the best of our knowledge, little work,

* Corresponding author. Tel.: +86 21 55664329; fax: +86 21 55664621.
** Corresponding author.
E-mail addresses: fyli@fudan.edu.cn (F. Li), chhuang@pku.edu.cn (C. Huang).

0378-7753/$ – see front matter © 2007 Elsevier B.V. All rights reserved.
doi:10.1016/j.jpowsour.2007.07.007

however, was reported to modify TiO_2 film for the same aim.

Generally, the reactions are more effective when the transport paths, through which molecules move into or out of the nanostructured materials, are included as an integral part of the architectural design [32,33]. Moreover, the liquid and quasi-solid/solid-state materials may more easily diffuse into the nanopores of the nanostructured materials through the suitable transport paths. These transport paths may be realized through a hierarchical combination of independently controlled, well-connected meso- and macro-pores [33]. It is well known that many mesoporous materials, such as hexagonal mesoporous silica [34] and TiO_2 [35–38], consist of smaller domain size with short channels and larger textural mesoporosity. Grätzel et al. [35] and our group [36] have investigated mesoporous TiO_2 films exhibiting greatly enhanced performance in DSSCs (with organic liquid electrolytes). Such mesoporous TiO_2 films are applicable for quasi-solid/solid-state DSSCs, but the performance of actual cells is limited by incomplete filling of mesopores due to the small pore size (<10 nm) [38]. Karthikeyan et al. [39] investigated the influence of three different nanocrystalline TiO_2 films, prepared from three different routes, namely sol–gel, thermal and colloidal-microwave process, on the performance of solid-state DSSCs. And they found that the optimal pore and morphological structures of TiO_2 film were important for efficient functioning of solid-state DSSCs, but the conversion efficiencies were low (<1%). Therefore, the design of TiO_2 film with more suitable meso- and macro-pores may be more beneficial to the improvement of the interfacial contact and reaction between the dye-coated TiO_2 film and the electrolyte. Herein, we reported a simple approach to prepare novel nanocrystalline TiO_2 films with the textural channels (micro-sized cracks on the surface and about 41 nm nanopores in the film bulk) via packaging ZnO nanowires into TiO_2 films and subsequently etching ZnO nanowires by hydrochloric acid. These textural channels in TiO_2 film enhanced the penetration of quasi-solid/solid-state electrolytes and therefore led to the obvious improvement of the performance of DSSCs.

2. Experimental

2.1. Materials

All the regents used were of analytical purity. Zn $(CH_3COO)_2{\cdot}2H_2O$, NaOH, KOH, ethanol, poly(ethylene glycol) (PEG, MW = 20,000), PEG (MW = 400), 2-propanol, acetone, $TiCl_4$, titanium butoxide, petroleum ether (60–90 °C) and hydrochloric acid were purchased from Sinopharm Chemical Reagent Corporation (China). Titanium tetraisopropoxide, I_2, LiI, *N*-methyl-benzimidazole (NMBI), polyethylene oxide (PEO, $M_w = 2 \times 10^6$), poly(vinylidene fluoride)(PVDF, $M_w = 1 \times 10^5$), 1,2-dimethoxyethane (DME) and poly(vinylidenefluoride-*co*-hexafluoropropylene) (PVDF-HFP) were obtained from Aldrich. TiO_2 nanoparticle (P25) and fumed silica nanoparticles (A380, 12-nm primary particles size) were purchased from Degussa. Propylene carbonate (PC) and 4-*tert*-butylpyridine were obtained from Acros. *cis*–bis(isothiocyanato) -bis(2,2′-bipyridyl-4,4′-dicarboxylato) ruthenium(II) (abbreviated as N3) was purchased from Solaronix (Switzerland). 1-Methyl-3-propylimidazolium iodide (MPII) was synthesized according to literature [40]. Transparent conductive oxide glass (TCO, F-doped SnO_2-coated glass, 85% transmittance in the visible, 15 Ω square^{-1}) was received as a gift from the General Electronics Company.

2.2. Preparation of nanocrystalline TiO_2 films without/with the textural channels

TCO glass substrates were immersed in a saturated solution of KOH in 2-propanol overnight, rinsed with acetone, ethanol and doubly deionized water successively, and dried in a nitrogen stream. To improve the ohmic contact and to avoid short circuiting and loss of current through recombination at TCO electrode, a compact (about 100 nm-thick) TiO_2 layer was first deposited onto TCO glass as follow [42]. TCO glass was dipped into the mixture of titanium butoxide and petroleum ether (2:98, v/v), taken out carefully, hydrolyzed in air for 30 min, and sintered in oven for 20 min at 450 °C.

ZnO nanowires with diameter of 30–50 nm and length of 0.5–2 μm were prepared according to the literature [41]. About 120 g/L TiO_2 colloidal dispersion, containing 40 wt.% poly(ethylene glycol) (MW = 20,000), was prepared by the hydrolysis of titanium tetraisopropoxide according to our previous report [3]. One hundred and sixty-five milligrams as-prepared ZnO nanowire was dispersed in 1 mL ethanol. Then this nanowire suspension was mixed with 10 mL TiO_2 colloidal dispersion and consequently stirred for over 2 days. Then several drops of TiO_2 colloidal dispersion containing ZnO nanowire was spread uniformly (using the doctor-blading technique) onto the top of the compact TiO_2 layer followed by annealing at 450 °C in air flow for 30 min. About 10-μm-thick novel TiO_2 films containing ZnO nanowire (denoted as ZnO–TiO_2 film) were obtained by repeating the above procedure several times. Acid treatment (etching ZnO nanowire) was carried out by soaking ZnO–TiO_2 film in 0.5 M hydrochloric acid at 75 °C for over 1 day. ZnO–TiO_2 films before and after the acid treatment were denoted as ZnO–TiO_2–BT and ZnO–TiO_2–AT, respectively. For comparison, 10-μm-thick traditional nanocrystalline TiO_2 films were prepared by using TiO_2 colloidal dispersion without any nanowire [3]. The traditional nanocrystalline TiO_2 films before and after the same acid treatment were denoted as TiO_2–BT and TiO_2–AT, respectively. After the acid treatment, all TiO_2 films were still strongly adherent to TCO glass substrates.

2.3. Construction of DSSCs based on nanocrystalline TiO_2 films without/with the textural channels

TiO_2–AT and ZnO–TiO_2–AT were soaked in the 0.2 M aqueous $TiCl_4$ solution overnight [2]. After being washed with deionized water, they were heated again at 450 °C for 30 min. Dye sensitization of these films was carried out by immersing the films (still warm, i.e., 80–100 °C) in ethanol solution containing 0.5 mM N3 dye for over 12 h. The N3-coated TiO_2 films

were dipped in 4-*tert*-butylpyridine for 15 min and then used as working electrode. The counter electrode was TCO glass on which 200 nm thick layer of Pt was deposited by sputtering. The electrodes were separated by a 40-μm-thick hot-melt ring (Surlyn 1702, DuPont).

In order to compare the performance of cell fabricated from two kinds of TiO_2 films, we selected an organic liquid electrolyte (Liquid-S0), two kinds of quasi-solid-state electrolytes (Quasi-solid-S1, Quasi-solid-S2) and a solid-state electrolyte (Solid-S3) as model electrolytes. Liquid-S0, composed of 0.03 M I_2 and 0.3 M LiI in propylene carbonate, was attracted into the inter-electrode space by capillary forces. Quasi-solid-S1 was the ionic liquid-based gel prepared by mixing fumed silica nanoparticles (5 wt.%) and the MPII solution containing 0.5 M I_2 and 0.45 M NMBI [15]. Quasi-solid-S2 was the ionic liquid polymer gel consisting of the solution (0.5 M I_2, 0.45 M NMBI in MPII) and PVDF–HFP (10 wt.%) [14]. Quasi-solid-S1 and Quasi-solid-S2 were injected into the sandwiched cells using a vacuum pump, respectively. Solid-S3 was the hybrid PEO/PVDF/TiO_2 nanoparticle solid-state electrolyte and prepared as follow [28]. The polymer-blend solution was composed of 0.080 g PEO and 0.012 g PVDF in 10.0 g the mixture of propylene carbonate and 1,2-dimethoxyethane (DME) (volume ratio = 7:3). Subsequently, 0.029 g TiO_2 nanoparticles (P25) and 2.0 mL the I^-/I_3^- redox-couple solution (dissolving 3.042 g LiI and 0.461 g I_2 in 30 mL acetonitrile) were added. At last, the above solution was coated onto the dye-coated TiO_2 film and heated to evaporate the solvent.

2.4. Characterization and photoelectrochemical measurement

X-ray diffraction (XRD) measurements were performed on a Bruker D4 X-ray diffractometer using Cu Kα radiation (λ = 0.15418 nm). The surface/cross section morphologies and the elements of the films were studied by field emission-scanning electron microscope (FE-SEM, JSM-6700F) with energy dispersive spectroscopy (EDS, Oxford INCA model 7421). Nitrogen adsorption/desorption isotherms were measured with a Micromeritics Tristar 3000 analyzer at 77 K. The Brunauer–Emmett–Teller (BET) method was utilized to calculate the surface areas. The total pore volume was estimated from the amount adsorbed at a relative pressure of 0.99. The pore size distributions were calculated from the adsorption branches using the Barrett–Joyner–Halenda (BJH) method. UV–vis absorption spectra of dye-coated films were collected using Shimadzu UV-2550 UV–vis-near infrared spectrophotometer with TCO substrate as a blank.

The photocurrent-density/voltage curves were measured in a two-electrode system under illumination (75 mW cm^{-2}) using a computerized Keithley Model 2400 SourceMeter unit. A 1000 W xenon lamp (Thermo Oriel, American) served as the light source. The active electrode area was typically 0.15 cm^2. The results are not corrected with respect to transmission losses in the conducting substrate. Monochromatic light in the range of 400–800 nm was obtained by using a series of filters, and the incident photo to current conversion efficiency (IPCE) measurement were performed on a Keithley Model 2400 SourceMeter.

Electrochemical impedance spectroscopy (EIS) measurements of the similar two-electrode system were performed with a Solartron SI 1287 electrochemical interface and a Solartron SI 1250 impedance/gain-phase analyzer. The spectra were obtained by applying sinusoidal perturbations of ±10 mV at frequencies from 10^{-2} to 10^5 Hz in the dark and under illumination (10 mW cm^{-2}). The obtained spectra were fitted with Z-View software (V2.70) in terms of appropriate equivalent circuits.

3. Results and discussion

3.1. Preparation and characterization of TiO_2 films

XRD patterns of traditional TiO_2 films and novel ZnO–TiO_2 films were investigated and shown in Fig. 1. There is no obvious difference in XRD patterns between TiO_2–BT and TiO_2–AT, so only XRD pattern of TiO_2–AT is given as shown in Fig. 1A. The diffraction peaks of TiO_2–AT are identified as belonging to both TiO_2 and polycrystalline SnO_2 (TCO glass substrate). The pattern associated with TiO_2 reveals a typical anatase structure in good agreement with anatase reference data. After packaging ZnO nanowires into TiO_2 film, the diffraction peaks associated with ZnO are also observed in the pattern of ZnO–TiO_2–BT, besides the diffraction peaks corresponding to TiO_2 with anatase structure. However, the pattern of ZnO–TiO_2–AT is very similar to that of TiO_2–AT, and the diffraction peaks corresponding to ZnO are not found, which indicates that ZnO nanowires have been removed effectively by the acid treatment. In addition, average TiO_2 crystalline sizes are estimated from the full width at half-maximum (FWHM) of the diffraction peak at 25.4° using Scherrer equation $D = 0.9\lambda/\beta \cos\theta$ (where D is the crystal size, λ the wavelength of X-ray radiation, β the full width at half maximum, and θ is the diffraction angle). The estimated TiO_2 particle sizes are about 14 nm for all films, regardless of the presence of ZnO and acid treatment.

The surface morphologies (low magnification) of TiO_2–BT and ZnO–TiO_2–BT were investigated by field emission-

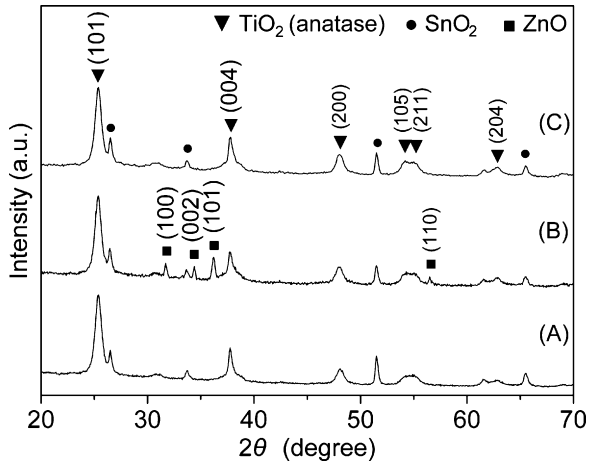

Fig. 1. XRD patterns of TiO_2–AT (A), ZnO–TiO_2–BT (B) and ZnO–TiO_2–AT (C).

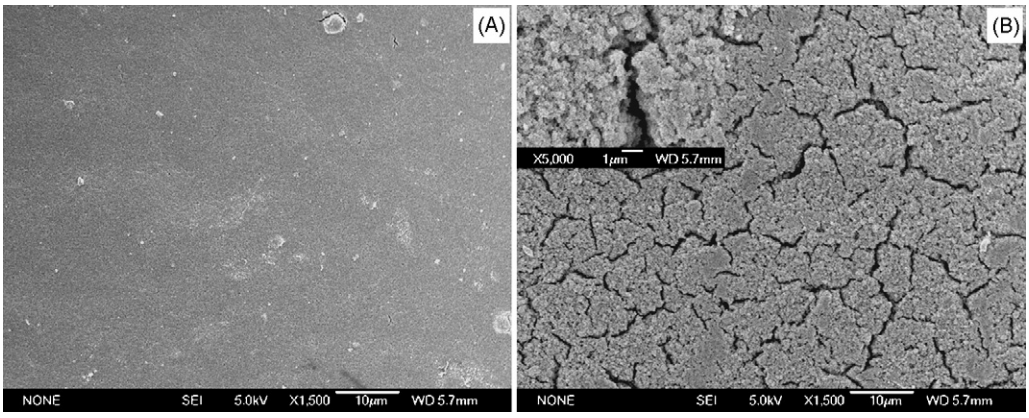

Fig. 2. The surface morphologies of TiO_2–BT (A) and ZnO–TiO_2–BT (B).

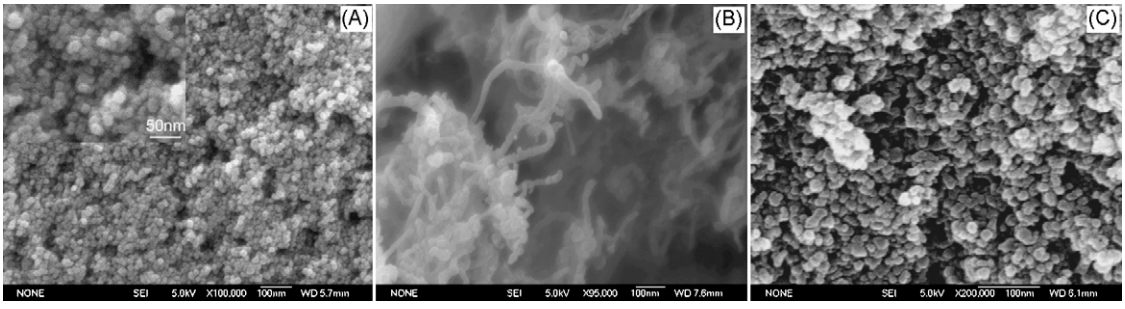

Fig. 3. FE-SEM micrographs showing cross section of TiO_2–AT (A), ZnO–TiO_2–BT (B) and ZnO–TiO_2–AT (C).

scanning electron microscope (FE-SEM) and shown in Fig. 2. Uniform and smooth surface with very little crack is found in TiO_2–BT (Fig. 2A). The surface morphology of TiO_2–AT is similar to that of TiO_2–BT. However, it is clear that there are plenty of cracks with 0.2–1.0 μm in width and about 10 μm in length on the surface of ZnO–TiO_2–BT (Fig. 2B). The depth of the cracks was further studied and found to be about 2 μm. Obviously, the cracks are mainly caused by the introduction of ZnO nanowire in ZnO–TiO_2–BT. It is deduced that the difference of expansion coefficient between TiO_2 and ZnO results in these cracks in ZnO–TiO_2–BT during the annealing process. Moreover, after the acid treatment, these cracks remain changeless in ZnO–TiO_2–AT. Electric measurement indicates that these cracks have no obvious adverse effect on the conductivity of ZnO–TiO_2–AT.

To further investigate the structure of both traditional TiO_2 film and ZnO–TiO_2 film, the cross sections of these films were studied by FE-SEM at higher magnification as shown in Fig. 3. No obvious effect of the acid treatment on the morphologies of traditional TiO_2 films is found, so only the cross section of TiO_2–AT is given (Fig. 3A). It is clear that TiO_2–AT is composed of a three-dimensional network of interconnected particles with the grain size between 10 and 20 nm. However, the addition of ZnO nanowires leads to a great change in the cross sections of ZnO–TiO_2–BT (Fig. 3B). Nanowires with diameter of about 40 nm are easily found and this cross section is very coarse due to the existence of nanowires. On the contrary, no nanowire is observed in ZnO–TiO_2–AT (Fig. 3C), suggesting that the acid treatment leads to the disappearance of ZnO nanowires in good agreement with XRD patterns. The composition of cross sections of ZnO–TiO_2–BT and ZnO–TiO_2–AT has also been analyzed by energy dispersive spectroscopy (EDS), and the results are shown in Fig. 4. It can be seen from Fig. 4A that ZnO–TiO_2–BT is composed of Ti, Zn and O element, besides Pt element (resulting from vacuum deposition of Pt to increase conductivity). After the acid treatment, Zn element disappears (Fig. 4B), which further confirms the removal of ZnO nanowire in ZnO–TiO_2–AT.

Importantly, as can be seen from Fig. 3(A) and (C), ZnO–TiO_2–AT has more and bigger nanopores than TiO_2–AT. To further investigate these nanopores, the nitrogen adsorption/desorption isotherms and pore size distribution curves of

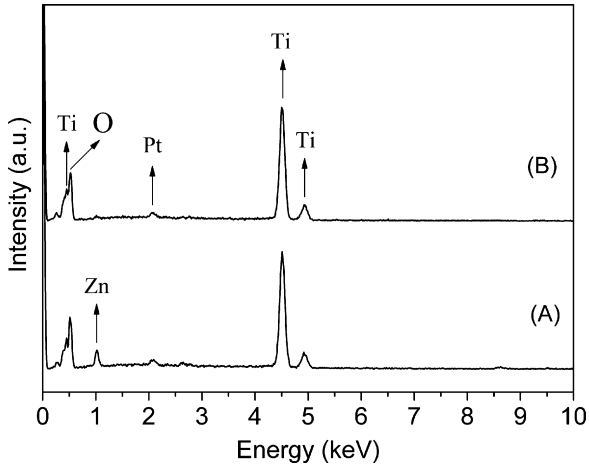

Fig. 4. EDS pattern of ZnO–TiO_2–BT (A) and ZnO–TiO_2–AT (B).

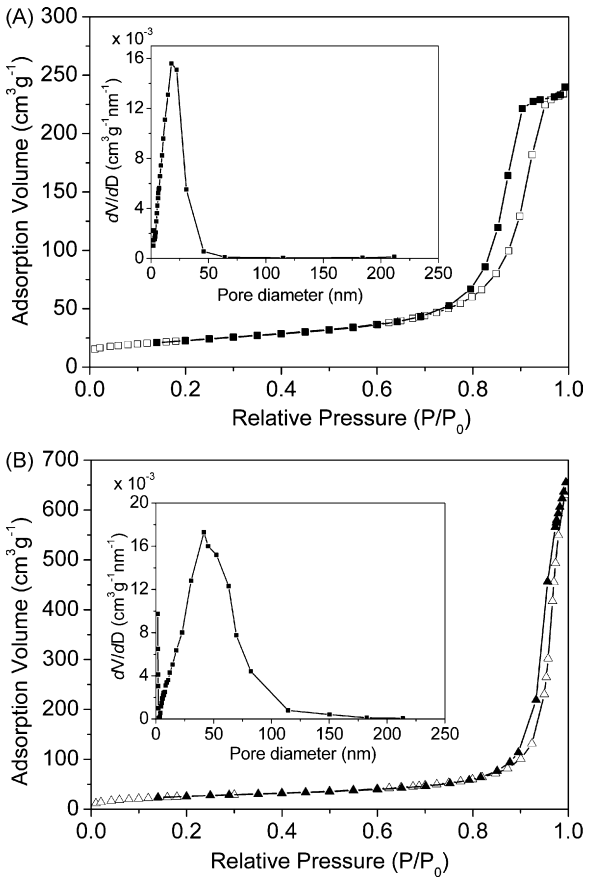

Fig. 5. Nitrogen sorption isotherms of TiO_2–AT (A) and ZnO–TiO_2–AT (B). Insets are BJH pore size distribution curves calculated from the adsorption branches.

both TiO_2–AT and ZnO–TiO_2–AT were measured and shown in Fig. 5. The pore size of TiO_2–AT is centered around 20 nm and the full width at half-maximum (FWHM) of the peak is about 20 nm (the inset of Fig. 5A). Interestingly, the maximum of the pore size of ZnO–TiO_2–AT is 41 nm (the inset of Fig. 5B) and the distribution of pore size for ZnO–TiO_2–AT is quite wider (FWHM of about 45 nm), which further confirm that plenty of bigger nanopores have been formed in ZnO–TiO_2–AT due to the removal of ZnO nanowires. It also can be deduced that some nanopores have the shapes replicated from the morphologies of their mother mold (ZnO nanowires). Such relatively wide nanopores in the film as well as the cracks on the surface can be considered as the textural channels. It can be expected that the textural channels in ZnO–TiO_2–AT are beneficial to the penetration of the quasi-solid/solid-state materials into the nanopores of films. Furthermore, pore volumes and BET surface areas are calculated according to the nitrogen adsorption/desorption isotherm. The pore volume of ZnO–TiO_2–AT (1.01 $cm^3\ g^{-1}$) is nearly tripled compared with that of TiO_2–AT (0.37 $cm^3\ g^{-1}$). Higher pore volume of ZnO–TiO_2–AT may be attributed to the following reason: (1) after the acid treatment, ZnO nanowires have been removed. As a result, the volume of ZnO nanowires contributes to the pore volume. (2) The accumulated pores constructed between ZnO nanowires and TiO_2 nanoparticles are usually higher than that constructed only from TiO_2 nanoparticles. (3) Plenty of ZnO nanowires may form some nano-architectures that supply bigger interspaces and therefore greatly improve the pore volume. (4) The presence of ZnO nanowires can prevent the densification of films and decrease density of TiO_2 nanoparticles, which also increase the pore volume. (5) The crack with in ZnO–TiO_2–AT may have contribution to the pore volume. In addition, BET surface area of ZnO–TiO_2–AT increases to 94.2 $m^2\ g^{-1}$ from 80.5 $m^2\ g^{-1}$ of TiO_2–AT. This slight increase originates from the presence of the textural channels instead of the change of grain size.

3.2. The performance of DSSCs based on TiO_2–AT and ZnO–TiO_2–AT

The changes of nanopores and pore volume of TiO_2 film may affect the performance of DSSCs. *I–V* measurements of DSSCs based on TiO_2–AT/ZnO–TiO_2–AT electrodes filled with an organic liquid electrolyte (Liquid-S0), two kinds of quasi-solid-state electrolytes (Quasi-solid-S1, Quasi-solid-S2) and a solid-state electrolyte (Solid-S3) were performed, respectively. The results under 75 mW cm^{-2} illumination in terms of open circuit voltage (V_{oc}), short circuit current density (J_{sc}), fill factor (ff), overall solar-to-electric energy conversion efficiencies (defined by $\eta = V_{oc}J_{sc}ff/I_{ph}$, where I_{ph} is the incident photon flux) and the improved ratio of η (defined by $y = (\eta ZnO\text{–}TiO_2\text{-AT} - \eta TiO_2\text{-AT})/\eta TiO_2\text{-AT} \times 100$) are presented in Table 1. When liquid electrolyte (Liquid-S0) is used, the conversion efficiency of DSSCs based on ZnO–TiO_2–AT (8.17%) increases only by 3.6% in contrast to that (7.88%) of TiO_2–AT system (Table 1). As mentioned above, phase structure, particle sizes and composition

Table 1
Comparison of the performance of DSSCs fabricated from TiO_2–AT electrode and ZnO–TiO_2–AT electrode (film thickness: about 10 μm)

Electrolyte	Film	V_{oc} (V)	J_{sc} (mA cm^{-2})	ff	η (%)	Improved ratio (y) (%)
Liquid-S0	TiO_2–AT	0.696	12.60	0.674	7.88	–
	ZnO–TiO_2–AT	0.699	13.10	0.669	8.17	3.6
Quasi-solid-S1	TiO_2–AT	0.658	8.58	0.662	4.98	–
	ZnO–TiO_2–AT	0.664	10.57	0.651	6.09	22.3
Quasi-solid-S2	TiO_2–AT	0.656	8.37	0.655	4.80	–
	ZnO–TiO_2–AT	0.667	10.14	0.639	5.76	20.2
Solid-S3	TiO_2–AT	0.663	8.13	0.565	4.06	–
	ZnO–TiO_2–AT	0.669	9.58	0.618	5.28	30.1

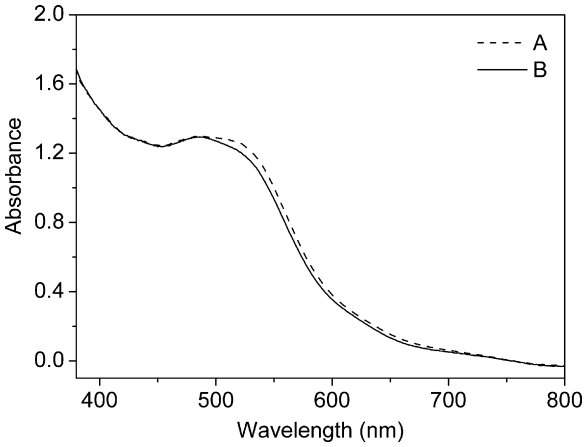

Fig. 6. UV–vis absorption spectra of the dye-coated ZnO–TiO_2–AT (A) and TiO_2–AT (B). Spectra are normalized to the absorbance at 400 nm.

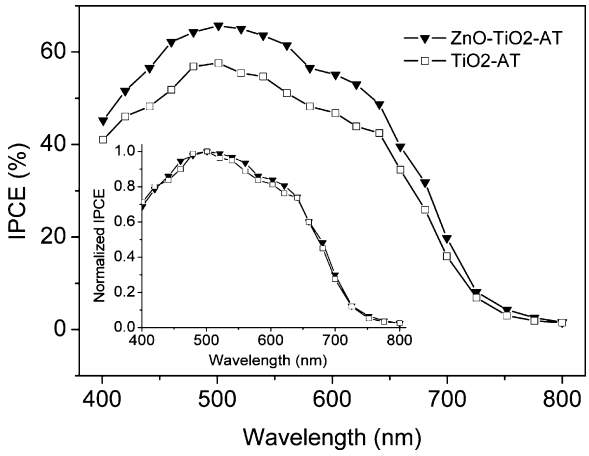

Fig. 7. IPCE spectra of DSSCs fabricated from ZnO–TiO_2–AT and TiO_2–AT electrode filled with Quasi-solid-S1. Inset is the normalized IPCE spectra.

of TiO_2–AT are as same as those of ZnO–TiO_2–AT. Generally, the penetration of organic liquid electrolyte into all nanocrystalline TiO_2 films is excellent. Therefore, it can be deduced that the slight improvement of J_{sc} for ZnO–TiO_2–AT system may result from some factors such as the mild increase of the BET surface area (from 80.5 $m^2\ g^{-1}$ for TiO_2–AT to 94.2 $m^2\ g^{-1}$ for ZnO–TiO_2–AT).

More importantly, for all DSSCs based on these quasi-solid/solid-state electrolytes (Quasi-solid-S1, Quasi-solid-S2, Solid-S3), the conversion efficiencies (η) from ZnO–TiO_2–AT electrodes are larger by 20–30% compared to those from TiO_2–AT electrodes (Table 1). The improvement chiefly results from the remarkable enhancement of short-circuit current density (J_{sc}). Here it cannot be deduced that the great enhancement of J_{sc} (and η) in quasi-solid/solid-state DSSCs based on ZnO–TiO_2–AT is decided by the increase of BET surface area. The main reasons for J_{sc} increase in ZnO–TiO_2–AT systems are investigated as follows.

It has been revealed experimentally and theoretically that by introducing large particles (several hundreds of nanometer) or spherical voids into TiO_2 film, the absorbance and IPCE values in longer wavelength range (especially 650–750 nm) can be greatly enhanced through light scattering, which can improve the cell performance [43–48]. In our case, UV–vis absorption spectrum of dye-coated ZnO–TiO_2–AT is similar to that of dye-coated TiO_2–AT as shown in Fig. 6, which indicates that no obvious light scattering can be observed, probably resulting from these facts that the average pore size (about 41 nm) of ZnO–TiO_2–AT is too small and that the micron-sized cracks on the surface is too large. The IPCE values of DSSCs based on both kinds of films filled with Quasi-solid-S1 are plotted *versus* wavelength in Fig. 7. ZnO–TiO_2–AT system shows better photoelectrical response, and the IPCE between 450 and 650 nm are much higher than that of TiO_2–AT system. On the other hand, the difference between the IPCE values of these two systems in longer wavelength range (especially 650–750 nm) is small as shown in the inset of Fig. 7, which further confirms the fact that the effect of light scattering on the cell performance is negligible. Therefore, the contribution of scattering effect for the J_{sc} (and η) improvement of ZnO–TiO_2–AT systems is minor. The main reasons for J_{sc} increase in ZnO–TiO_2–AT systems may be the improvement of the interfacial contact and reaction between the dye-coated TiO_2 film and the electrolyte, which are further studied by FE-SEM and electrochemical impedance spectroscopy (EIS) technique.

The interfacial contact between the dye-coated TiO_2 film and the electrolyte is dependent on the penetration of the electrolyte into the nanopores of the film. The pore filling of the nanoporous TiO_2 layer by quasi-solid/solid-state electrolytes (Quasi-solid-S1, Quasi-solid-S2, Solid-S3) were investigated by FE-SEM. Fig. 8 shows cross-section FE-SEM micrographs of TiO_2–AT and ZnO–TiO_2–AT electrodes filled with Quasi-solid-S1. Although the image of the nanoparticles in TiO_2–AT electrode is indistinct (Fig. 8A), we still can distinguish nanoparticles, which reveals that the nanopores of TiO_2–AT is not completely filled. Interestingly, the cross-section (Fig. 8B) of ZnO–TiO_2–AT electrode is apparently smooth and homogeneous, and no typical TiO_2 nanoparticle is observed, which suggests that TiO_2 particles are completely covered by Quasi-solid-S1 and the pore filling is excellent. The penetration phenomena of Quasi-solid-S2 and Solid-S3 are similar to that of Quasi-solid-S1. These facts suggest that ZnO–TiO_2–AT system exhibits better pore filling by quasi-solid/solid-state electrolytes than TiO_2–AT system, which will result in better interfacial contact in ZnO–TiO_2–AT system.

Electrochemical impedance spectroscopy (EIS) technique has been widely employed to study the kinetics of electrochemical and photoelectrochemical processes occurring in DSSCs [49–53]. We also investigated the effect of the textural channels on the interface and kinetics in DSSCs by EIS technique. The impedance spectra of DSSCs based on TiO_2–AT and ZnO–TiO_2–AT filled with Quasi-solid-S1 were measured at open circuit voltage (OCV, −0.68 V) under illumination and under forward bias (−0.68 V) in the dark [49]. The results are shown in Fig. 9. Experimental data are represented by symbols while the solid lines correspond to the fit obtained with Z-View software using the equivalent circuit shown in Fig. 10. Parameters obtained by fitting the experimental spectra with

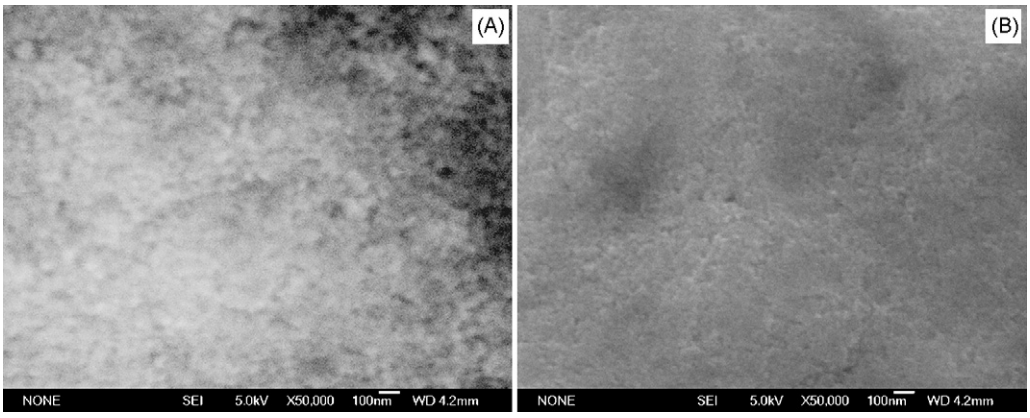

Fig. 8. Cross-section FE-SEM micrographs of TiO_2–AT electrode (A) and ZnO–TiO_2–AT electrode (B) filled with electrolyte S1 (TiO_2 film depth: ~6 μm).

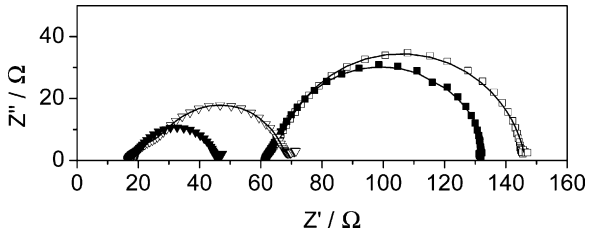

Fig. 9. Impedance spectra of DSSCs based on TiO_2–AT and ZnO–TiO_2–AT filled with Quasi-solid-S1. TiO_2–AT system in the dark (□) and under illumination (■), ZnO–TiO_2–AT system in the dark (▽) and under illumination (▼).

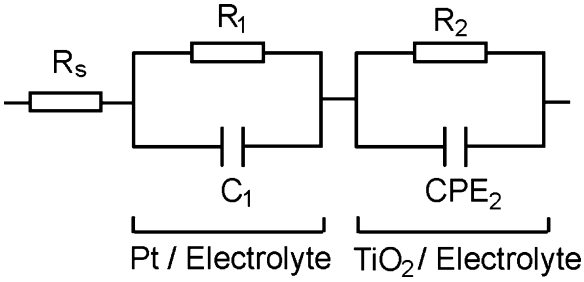

Fig. 10. Equivalent circuit of DSSCs.

this equivalent circuit in the frequency ranging from 0.1 to 8×10^4 Hz are shown in Table 2.

The impedance spectra of TiO_2–AT system are similar to that of ZnO–TiO_2–AT system. All spectra exhibit a large semicircle at low frequencies and a small one at high frequencies, which are fitted with a $R_S(R_1C_1)(R_2CPE_2)$ equivalent circuit similar to literature [50,52]. In general, a constant phase element (CPE) is used in the model in place of a capacitor to compensate for inhomogeneity in the system. In the Z-View software, the CPE is defined by two parameters, the value (CPE-T) of capacitance of the CPE element and the change (CPE-P) of the compressed semicircle from an ideal semicircle. The frequency range and the size of the small semicircle (associated with R_1 and C_1 element) suggest that such semicircle is associated with kinetic processes at the Pt counter electrode [50,51]. The low frequency (large) semicircle (associated with R_2 and CPE_2 element) is correlated with the photoelectrode, taking into account the charge-transfer process that occurs across the TiO_2 | redox electrolyte. Both in the dark and under illumination, ZnO–TiO_2–AT systems exhibit lower values for R_2 resistance and higher values for the CPE_2 capacitance (associated with CPE_2-T parameter) than the analogous components of TiO_2–AT system (Table 2), implying more efficient charge-transfer process at the dye-coated ZnO–TiO_2–AT | electrolyte interface (reduction of oxidized dye by I^-). Furthermore, the impedance at high frequency, associated to the R_S element, is 61–62 Ω for TiO_2–AT system and 17–19 Ω for ZnO–TiO_2–AT system (Table 2). Usually, the R_S element is related to the series resistance of the electrolyte and electrical contacts in an electrochemical cell. For such solar cells, the R_S component can account not only for resistance of the electrolyte, but also for the resistance within the TiO_2 film [52]. The lower R_S values observed for ZnO–TiO_2–AT system also reveal better electrical contact and thus more rapid ionic transfer in this device.

Based on the above results, the sketch of quasi-solid/solid-state DSSCs fabricated from ZnO–TiO_2–AT is simulated in Fig. 11. Obviously, the textural channels (micron-sized cracks and the nanopores with diameter of about 41 nm) in ZnO–TiO_2–AT are relatively wider and straighter than the aboriginal nanopores (diameter of about 20 nm) in TiO_2–AT. The

Table 2
Parameters obtained by fitting the impedance spectra of DSSCs fabricated from TiO_2–AT and Zn–TiO_2–AT filled with Quasi-solid-S1

Film	Condition	R_s (Ω)	C_1 (μF)	R_1 (Ω)	CPE_2-T (μF)	CPE_2-P	R_2 (Ω)
TiO_2–AT	Dark	62	14	4	45	0.89	81
	Illumination	61	16	3	44	0.90	70
Zn–TiO_2–AT	Dark	19	6	6	60	0.86	44
	Illumination	17	6	3	62	0.87	26

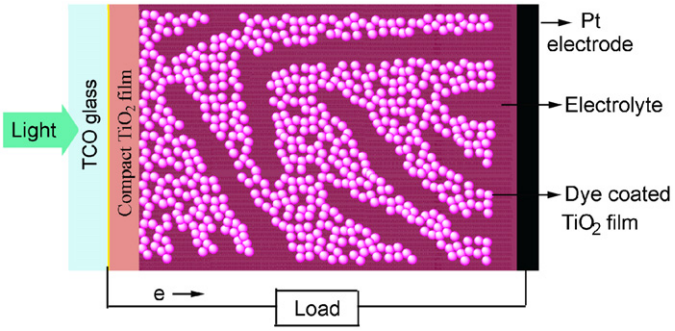

Fig. 11. Sketch of DSSCs based on ZnO–TiO_2–AT.

electrolytes more easily enter the deep layer of ZnO–TiO_2–AT through the textural channels when they are coated onto the surface of ZnO–TiO_2–AT, which leads to better effects of wetting and pore filling and thus better interfacial contact. Better interfacial contact, confirmed by better electrical contact (lower R_2 resistance and higher CPE_2 capacitance), results in more efficient interfacial reaction (reduction of oxidized dye by I^-) and thus higher photocurrent. In addition, plenty of electrolytes efficiently enter the textural channel with suitable pore size due to the complete pore filling of ZnO–TiO_2–AT system. Rolison [32] reported that the transport of small molecules in media featuring large mesopores (>10 nm) and macropores (>50 nm) can approach rates of diffusion comparable to those in open medium. We also believe that the transport of molecules or ions (I^-, I_3^-) in the textural channel filled with the electrolytes is very rapid. It even can be thought that for ZnO–TiO_2–AT system, ions have been equivalently transferred to the electrode surface when they are transferred to the textural channel filled with the electrolytes. This rapid transport of ions in ZnO–TiO_2–AT system is confirmed by lower value of R_S. More rapid transport of ions makes the interfacial reaction more effective and thus greatly improves the photocurrent. In brief, most improvement of the cell performance should be attributed to the presence of the textural channel.

4. Conclusions

TiO_2 films with the textural channels are obtained for the first time by a simply way. The presence of textural channels facilitates the penetration of quasi-solid/solid-state electrolytes into TiO_2 film and therefore leads to the great improvement (20–30%) of overall solar-to-electric energy conversion efficiencies. Further improvement can be expected if the channel in TiO_2 film is fine-tuned, for example, by varying the type, diameter and length of nanowire or aligning nanowire. More importantly, the new concept established here will be very helpful in developing other types of TiO_2 film for quasi-solid or solid-state DSSCs.

Acknowledgements

The authors thank Huo Yingdong Education Foundation (104012), National Science Foundation of China (20490210 and 20501006) and Shanghai Sci. Tech. Commun. (05DJ14004 and 06QH14002) for financial support.

References

[1] B. O'Regen, M. Grätzel, Nature 353 (1991) 737–740.
[2] M.K. Nazeeruddin, A. Kay, I. Rodicio, R. Humpbry-Baker, E. Müller, P. Liska, N. Vlachopoulos, M. Grätzel, J. Am. Chem. Soc. 115 (1993) 6382–6390.
[3] Z.S. Wang, F.Y. Li, C.H. Huang, L. Wang, M. Wei, L.P. Jin, N.Q. Li, J. Phys. Chem. B 104 (2000) 9676–9682.
[4] Z.G. Chen, Y.W. Tang, L.S. Zhang, L.J. Luo, Electrochim. Acta 51 (2006) 5870–5875.
[5] K. Hara, M. Kurashige, S. Ito, A. Shinpo, S. Suga, K. Sayama, H. Arakawa, Chem. Commun. (2003) 252–253.
[6] P. Ravirajan, A.M. Peiro, M.K. Nazeeruddin, M. Grätzel, D.D.C. Bradley, J.R. Durrant, J. Nelson, J. Phys. Chem. B 110 (2006) 7635–7639.
[7] H.X. Wang, H. Li, B.F. Xue, Z.X. Wang, Q.B. Meng, L.Q. Chen, J. Am. Chem. Soc. 127 (2005) 6394–6401.
[8] M. Grätzel, J. Photochem. Photobiol. A 164 (2004) 3–14.
[9] G.R.A. Kumara, A. Konno, K. Shiratsuchi, J. Tsukaraha, K. Tennakone, Chem. Mater. 14 (2002) 954–955.
[10] L. Schmidt-Mende, U. Bach, R. Humphry-Baker, T. Horiuchi, H. Miura, S. Ito, S. Uchida, M. Grätzel, Adv. Mater. 17 (2005) 813–815.
[11] U. Bach, D. Lupo, P. Comte, J.E. Moser, F. Weissörtel, J. Salbeck, H. Spreitzer, M. Grätzel, Nature 395 (1998) 583–585.
[12] W. Kubo, K. Murakoshi, T. Kitamura, S. Yoshida, M. Haruki, K. Hanabusa, H. Shirai, Y. Wada, S. Yanagida, J. Phys. Chem. B 105 (2001) 12809–12815.
[13] Z.G. Chen, F.Y. Li, H. Yang, T. Yi, C.H. Huang, ChemPhysChem 8 (2007) 1293–1297.
[14] P. Wang, S.M. Zakeeruddin, I. Exnar, M. Grätzel, Chem. Commun. (2002) 2972–2973.
[15] P. Wang, S.M. Zakeeruddin, P. Comte, I. Exnar, M. Grätzel, J. Am. Chem. Soc. 125 (2003) 1166–1167.
[16] H. Yang, C.Z. Yu, Q.L. Song, Y.Y. Xia, F.Y. Li, Z.G. Chen, X.H. Li, T. Yi, C.H. Huang, Chem. Mater. 18 (2006) 5173–5177.
[17] P. Wang, S.M. Zakeeruddin, J.E. Moser, M.K. Nazeeruddin, T. Sekiguchi, M. Grätzel, Nat. Mater. 2 (2003) 402–407.
[18] J.B. Xia, F.Y. Li, C.H. Huang, J. Zhai, L. Jiang, Sol. Energy Mater. Sol. Cells 90 (2006) 944–952.
[19] D.W. Kima, Y.B. Jeong, S.H. Kima, D.Y. Lee, J.S. Song, J. Power Sources 149 (2005) 112–116.
[20] X. Zhang, H. Yang, H.M. Xiong, F.Y. Li, Y.Y. Xia, J. Power Sources 160 (2006) 1451–1455.
[21] Z. Lan, J.H. Wu, J.M. Lin, M.L. Huang, J. Power Sources 164 (2007) 921–925.
[22] F.J. Li, F.Y. Cheng, J.F. Shi, F.S. Cai, M. Liang, J. Chen, J. Power Sources 165 (2007) 911–915.
[23] Q. Dai, D.R. MacFarlane, P.C. Howlett, M. Forsyth, Angew. Chem. Int. Ed. 44 (2005) 313–316.
[24] P. Wang, Q. Dai, S.M. Zakeeruddin, M. Forsyth, D.R. MacFarlane, M. Grätzel, J. Am. Chem. Soc. 126 (2004) 13590–13591.
[25] Z.G. Chen, H. Yang, X.H. Li, F.Y. Li, T. Yi, C.H. Huang, J. Mater. Chem. 17 (2007) 1602–1607.
[26] J.H. Kim, M.-S. Kang, Y.J. Kim, J. Won, N.-G. Park, Y.S. Kang, Chem. Commun. (2004) 1662–1663.
[27] M.-S. Kang, J.H. Kim, Y.J. Kim, J. Won, N.-G. Park, Y.S. Kang, Chem. Commun. (2005) 889–891.
[28] H.W. Han, W. Liu, J. Zhang, X.Z. Zhao, Adv. Funct. Mater 15 (2005) 1940–1945.
[29] R. Kumar, A.K. Sharma, V.S. Parmar, A.C. Watterson, K.G. Chittibabu, J. Kumar, L.A. Samuelson, Chem. Mater. 16 (2004) 4841–4846.
[30] T. Stergiopoulos, I.M. Arabatzis, G. Katsaros, P. Falaras, Nano Lett. 2 (2002) 1259–1261.
[31] L. Schmidt-Mende, M. Grätzel, Thin Solid Films 500 (2006) 296–301.
[32] D.R. Rolison, Science 299 (2003) 1698–1701.
[33] L.Z. Zhang, J.C. Yu, Chem. Commun. (2003) 2078–2079.
[34] D.Y. Zhao, J.L. Feng, Q.S. Huo, N. Melosh, G.H. Fredrickson, B.F. Chmelka, G.D. Stucky, Science 279 (1998) 548–552.
[35] M. Zukalova, A. Zukal, L. Kavan, M.K. Nazeeruddin, P. Liska, M. Grätzel, Nano Lett. 5 (2005) 1789–1792.

[36] K. Hou, B.Z. Tian, F.Y. Li, Z.Q. Bian, D.Y. Zhao, C.H. Huang, J. Mater. Chem. 15 (2005) 2414–2420.
[37] Y.Q. Wang, S.G. Chen, X.H. Tang, O. Palchik, A. Zaban, Y. Koltypin, A. Gedanken, J. Mater. Chem. 11 (2001) 521–526.
[38] K.M. Coakley, Y.X. Liu, M.D. McGehee, K.L. Frindell, G.D. Stucky, Adv. Funct. Mater. 13 (2003) 301–306.
[39] C.S. Karthikeyan, M. Thelakkat, M. Willert-Porada, Thin Solid Films 511–512 (2006) 187–194.
[40] P. Bonhte, A.P. Dias, M. Armand, N. Papageorgiou, K. Kalyanasudaram, M. Grätzel, Inorg. Chem. 35 (1996) 1168–1178.
[41] Z. Li, Y. Xiong, Y. Xie, Inorg. Chem. 42 (2003) 8105–8109.
[42] B. Li, L.D. Wang, D.Q. Zhang, Y. Qiu, Chin. Sci. Bull. 49 (2004) 123–127.
[43] A. Usami, Chem. Phys. Lett. 277 (1997) 105–108.
[44] A. Usami, Sol. Energy Mater. Sol. Cells 64 (2000) 73–83.
[45] S. Nishimura, N. Abrams, B.A. Lewis, L.I. Halaoui, T.E. Mallouk, K.D. Benkstein, J. van de Lagemaat, A.J. Frank, J. Am. Chem. Soc. 125 (2003) 6306–6310.
[46] W.E. Vargas, G.A. Niklasson, Sol. Energy Mater. Sol. Cells 69 (2001) 147–163.
[47] Y. Chiba, A. Islam, R. Komiya, N. Koide, L. Han, Appl. Phys. Lett. 88 (2006) 223505–223507.
[48] L.I. Halaoui, N.M. Abrams, T.E. Mallouk, J. Phys. Chem. B 109 (2005) 6334–6342.
[49] Q. Wang, J.-E. Moser, M. Grätzel, J. Phys. Chem. B 109 (2005) 14945–14953.
[50] J. van de Lagemaat, N.-G. Park, A.J. Frank, J. Phys. Chem. B 104 (2000) 2044–2052.
[51] N. Papageorgiou, W.F. Maier, M. Grätzel, J. Electrochem. Soc. 144 (1997) 876–884.
[52] C. Longo, A.F. Nogueira, M.-A. De Paoli, H. Cachet, J. Phys. Chem. B 106 (2002) 5925–5930.
[53] L. Han, N. Koide, Y. Chiba, T. Mitate, Appl. Phys. Lett. 84 (2004) 2433–2435.